Available online at www.sciencedirect.com
ScienceDirect
Journal of Solid State Chemistry 180 (2007) 1852–1862
JOURNAL OF SOLID STATE CHEMISTRY
www.elsevier.com/locate/jssc

Luminescent zinc and cadmium complexes incorporating 1,3,5-benzenetricarboxylate and a protonated kinked organodiimine: From a hydrogen-bonded layer motif to thermally robust two-dimensional coordination polymers

Maxwell A. Braverman[a], Ronald M. Supkowski[b], Robert L. LaDuca[a,*]

[a]*Lyman Briggs School of Science and Department of Chemistry, Michigan State University, E-30 Holmes Hall, East Lansing, MI 48825, USA*
[b]*Department of Chemistry and Physics, King's College, Wilkes-Barre, PA 18711, USA*

Received 7 March 2007; received in revised form 12 April 2007; accepted 16 April 2007
Available online 25 April 2007

Abstract

Hydrothermal treatment of zinc chloride, 1,3,5-benzenetricarboxylic acid (H_3BTC), and 4,4′-dipyridylamine (dpa) afforded two different complexes depending on reaction conditions, which were characterized by single-crystal X-ray diffraction, infrared spectroscopy, and elemental analysis. Under acidic conditions, a discrete neutral molecular species with formulation $[Zn(HBTC)_2(Hdpa)_2]$ (**1**) was isolated, which aggregates into two-dimensional hydrogen-bonded layers. Under more basic conditions, the two-dimensional layered coordination polymer [Zn(BTC)(Hdpa)] (**2**) is obtained, which manifests covalent linkage of [Zn(BTC)(Hdpa)] serpentine chain motifs into 3-connected undulating 4.8^2 topology 2-D layers. Both **1** and **2** possess tetrahedral coordination at Zn. Use of cadmium nitrate in the synthesis resulted in $[Cd(BTC)(H_2O)(Hdpa)]$ (**3**), which displays a similar layer topology as **2** but with significant adjustments imparted by octahedral coordination at Cd. In all cases, supramolecular hydrogen bonding promoted by Hdpa ligands provide an important assistive structure-directing role. All materials display blue luminescence upon excitation with ultraviolet light, ascribed to intraligand transitions. Crystallographic data: **1**: monoclinic, $C2/c$, $a = 25.389(6)$ Å, $b = 9.811(2)$ Å, $c = 17.309(4)$ Å, and $\beta = 128.957(3)^\circ$, **2**: monoclinic, $P2_1/c$, $a = 13.212(17)$c, $b = 17.15(2)$ Å, $c = 7.506(10)$ Å, and $\beta = 93.71(2)^\circ$, and **3**: monoclinic, $C2/c$, $a = 14.241(6)$ Å, $b = 15.218(6)$ Å, $c = 17.976(7)$ Å, and $\beta = 109.330(6)^\circ$.

Keywords: Coordination polymer; Zinc; Cadmium; Benzenetricarboxylate; Dipyridylamine; Crystal structure; Thermogravimetric analysis

1. Introduction

While their systematic study dates back approximately 15 years, metal-organic framework (MOF) materials remain an active focus of research due to their significant potential in diverse applications such as hydrogen storage [1], shape-selective separations [2], ion exchange [3], catalysis [4], non-linear optics [5], and luminescence [5]. Divalent d^{10} metal 1,3,5-benzenetricarboxylate (BTC) coordination polymers have proven to be an especially fruitful MOF system, displaying intriguing properties including microporosity [6], reversible crystal-to-amorphous phase transitions [7], functional-group selective adsorption [7,8], and photoluminescence [9]. The tremendous structural diversity uncovered in this MOF system hangs in part on the wide variety of accessible carboxylate binding modes (from monodentate to exohexadentate) and protonation levels, as well as numerous possible supramolecular interaction pathways including hydrogen bonding and π–π stacking [6–9]. In addition, the coordination geometry flexibility at d^{10} divalent Zn or Cd ions imparted by their lack of crystal field stabilization allows the local steric environment of the carboxylate ligand to play a very large role in structure direction. Tetrahedral, square pyramidal, trigonal bipyramidal, and octahedral coordination have all been observed in zinc BTC coordination polymers, while six- to seven-coordinate complexes have been reported for cadmium BTC MOF systems [6–9].

*Corresponding author.
E-mail address: laduca@msu.edu (R.L. LaDuca).

0022-4596/$ - see front matter © 2007 Elsevier Inc. All rights reserved.
doi:10.1016/j.jssc.2007.04.010

More recently, the level of structural complexity in this system has been elevated by the inclusion of organodiimine co-ligands. Use of chelating imines such as 2,2′-bipyridine (2,2′-bpy) [10–12] or exobidentate rigid or flexible tethers such as 4,4′-bipyridine (4,4′-bpy) [13,14] or 1,3-di-4-pyridylpropane (dpp) [15] has allowed access to MOFs with previously unseen structure types. Many of these materials manifest interesting properties such as pH-dependent supramolecular isomerism [12,14] and non-linear optical and photoluminescent behavior [15]. It is clear that judicious variance of the organodiimine component can foster continued structural elaboration within zinc/BTC or cadmium/BTC coordination polymers.

For some time we have aimed our research efforts towards the characterization of coordination polymers containing the organodiimine 4,4′-dipyridylamine (dpa). In contrast to 4,4′-bpy, dpa possesses a kinked disposition of its nitrogen donor atoms due to its central amine, which also serves as a potential hydrogen bonding point of contact. The dpa ligand therefore can cause coordination polymer subunits to aggregate via supramolecular interactions as well as covalent bonding. Taking full advantage of the dual functionality of this ligand, we have been able to prepare several carboxylate and oxide MOFs with diverse structural motifs [16–18]. For example, $\{[Ni(dpa)_2(succinate)_{0.5}]Cl\}$ forms a unique 5-connected 3-D self-penetrated framework [16], $[Mo_4O_{13}(Hdpa)_2]$ possesses unprecedented interdigitated 1-D molybdate ribbons that can intercalate primary and secondary amines [17], and $[NiMoO_4(dpa)_2]$ has a "starburst" 3-D structure formed by the linkage of cationic $[Ni(dpa)_2]^{2n+}$ layers through molybdate tetrahedra [18]. Hanton has recently extended the coordination chemistry of dpa into silver, copper, and cadmium oxoanion systems, revealing the ability of dpa to impart chirality by acting as a "double-bladed propeller" [19]. We report here the preparation and characterization of the first benzenetricarboxylate complexes to incorporate the dpa ligand. In the zinc case, the pH of the initial reaction mixture causes toggling between a "zero-dimensional" molecular species and an undulating 3-connected two-dimensional slab coordination polymer displaying high thermal stability. A different 3-connected two-dimensional slab pattern is observed in the cadmium case due to its altered coordination geometry. In all three materials, significant supramolecular interactions promoted by the dipyridylamine subunit serve an assistive role in structure direction. Thermal and luminescent properties of these materials are also described herein.

2. Experimental section

2.1. General considerations

$ZnCl_2$, $Cd(NO_3)_2 \cdot 4H_2O$ and 1,3,5-benzenetricarboxylic acid (H_3BTC) (Aldrich) were obtained commercially. dpa was prepared via a published procedure [17]. Water was deionized above 3 MΩ in-house. Thermogravimetric analysis was performed on a TA Instruments TGA 2050 Thermogravimetric Analyzer with a heating rate of 10 °C min^{-1}. Elemental analysis was carried out using a Perkin Elmer 2400 Series II CHNS/O Analyzer. IR spectra were recorded on powdered samples on a Perkin Elmer Spectrum One instrument. Luminescence spectra were recorded with a Spex Fluorolog spectrometer, using crystalline solid-state samples anchored to quartz slides using Rexon RX-22P ultraviolet-transparent epoxy.

2.2. Preparation of $[Zn(HBTC)_2(Hdpa)_2]$ (1)

$ZnCl_2$ (75 mg, 0.55 mmol), dpa (96 mg, 0.56 mmol), and H_3BTC (156 mg, 0.74 mmol) were added to 10 mL of distilled H_2O in a 23 mL Teflon-lined Parr acid digestion bomb. The pH level was adjusted to 4.7 with 0.6 mL of 1.0 M aqueous HCl. The bomb was sealed, heated to 120 °C for 48 h, and then gradually cooled to 23 °C. The final reaction mixture had a pH of 4.3. Colorless blocks of **1** (132 mg, 57% yield based on dpa) were obtained after filtration, washing with distilled water and acetone, and drying in air. Crystals of **1** were stable indefinitely in air. Synthetic experiments with $ZnCl_2$, dpa, and BTC in a 1:2:2 molar ratio resulted in a diminished yield of product. Anal. Calc. for $C_{38}H_{28}N_6O_{12}Zn$ **1**: C, 55.25; H, 3.42; N, 10.17%; Found: C, 54.56; H, 3.49; N, 10.21%. IR (KBr, cm^{-1}): 3316 w, 3143 w, 3043 m br, 1716 s, 1654 m, 1616 s, 1583 m, 1532 s, 1490 m, 1358 s, 1251 m, 1215 m, 1190 m, 1080 m, 1031 m, 912 w, 824 m, 746 m, 724 m, 710 m, 680 w, 551 m, 480 w.

2.3. Preparation of $[Zn(BTC)(Hdpa)]$ (2)

$ZnCl_2$ (50 mg, 0.37 mmol), dpa (64 mg, 0.37 mmol), and H_3BTC (78 mg, 0.37 mmol) were added to 10 mL of distilled H_2O in a 23 mL Teflon-lined Parr acid digestion bomb. The pH level was adjusted to 11.5 with 1.0 mL of 1.0 M aqueous NaOH. The bomb was sealed, heated to 120 °C for 24 h, and then gradually cooled to 23 °C. The final reaction mixture had a pH of 5.3. Colorless blocks of **2** (112 mg, 67% yield) were obtained after filtration, washing with distilled water and acetone, and drying in air. Crystals of **2** were stable indefinitely in air. Anal. Calc. for $C_{19}H_{13}N_3O_6Zn$ **2**: C, 51.31; H, 2.95; N, 9.45%; Found: C, 50.85; H, 3.00; N, 9.43%. IR (KBr, cm^{-1}): 3400 w br, 3000 m br, 1624 s, 1550 m, 1540 m, 1517 s, 1439 s, 1358 s, 1229 m, 1185 m, 1100 w, 1082 w, 1037 w, 897 w, 872 w, 824 m, 795 m, 724 m, 647 w, 566 w, 536 m, 462 w.

2.4. Preparation of $[Cd(BTC)(H_2O)(Hdpa)]$ (3)

$Cd(NO_3)_2 \cdot 4H_2O$ (145 mg, 0.33 mmol), dpa (127 mg, 0.74 mmol), and H_3BTC (78 mg, 0.33 mmol) were added to 10 mL of distilled H_2O in a 23 mL Teflon-lined Parr acid digestion bomb. The pH level was adjusted to 11.5 with 1.0 mL of 1.0 M aqueous NaOH. The bomb was sealed, heated to 120 °C for 26 h, and then gradually cooled to

23 °C. The final reaction mixture had a pH value of 5.3. Colorless blocks of **3** (128 mg, 76% yield based on Cd) were obtained after filtration, washing with distilled water and acetone, and drying in air. Crystals of **3** were stable indefinitely in air. Anal. Calc. for $C_{19}H_{15}CdN_3O_7$ **3**: C, 44.77; H, 2.97; N, 8.24%; Found: C, 44.51; H, 2.84; N, 8.13%. IR (KBr, cm^{-1}): 3323 w br, 2900 w br, 1640 w, 1605 s, 1575 w, 1539 w, 1510 s, 1481 w, 1438 m, 1357 s, 1204 m, 1096 w, 1013 m, 931 w, 870 w, 846 w, 820 s, 758 s, 726 s, 710 s, 688 w.

3. X-ray crystallography

A colorless block of **1** (0.25 mm × 0.20 mm × 0.20 mm), a colorless block of **2** (with dimensions 0.50 mm × 0.40 mm × 0.10 mm), and a colorless block of **3** (with dimensions 0.40 mm × 0.20 mm × 0.20 mm) were subjected to single-crystal X-ray diffraction using a Bruker-AXS SMART 1k CCD instrument at 293(2) K. Reflection data were acquired using graphite-monochromated Mo$K\alpha$ radiation ($\lambda = 0.71073$ Å). The data were integrated via SAINT [20]. Lorentz and polarization effect and empirical absorption corrections were applied with SADABS [21]. The structures were solved using direct methods and refined on F^2 using SHELXTL [22]. All non-hydrogen atoms were refined anisotropically. Hydrogen atoms bound to carbon atoms were placed in calculated positions and refined isotropically with a riding model. The hydrogen atoms bound to the dpa moieties in **1**–**3**, the protonated carboxylate oxygen in **1** and the aquo ligand in **3** were found via Fourier difference maps, restrained at fixed positions, and then refined isotropically with 1.2U(eq) of the N or O atoms to which they are bound. Relevant crystallographic data for **1**–**3** are listed in Table 1.

Table 1
Crystal and structure refinement data for **1**–**3**

Data	**1**	**2**	**3**
Empirical formula	$C_{38}H_{28}N_6O_{12}Zn$	$C_{19}H_{13}N_3O_6Zn$	$C_{19}H_{15}CdN_3O_7$
Formula weight	826.04	444.69	509.74
Collection T (K)	293(2)	293(2)	293(2)
λ (Å)	0.71073	0.71073	0.71073
Crystal system	Monoclinic	Monoclinic	Monoclinic
Space group	$C2/c$	$P2_1/c$	$C2/c$
a (Å)	25.389(6)	13.212(17)	14.241(6)
b (Å)	9.811(2)	17.15(2)	15.218(6)
c (Å)	17.309(4)	7.506(10)	17.976(7)
β (deg)	128.957(3)	93.71(2)	109.330(6)
V (Å^3)	3353.0(4)	1697(4)	3676(3)
Z	4	4	8
D_{calc} (g cm^{-3})	1.636	1.740	1.842
μ (mm^{-1})	0.814	1.494	1.239
Min/max T	0.962	0.792	0.787
hkl ranges	$-32\leqslant h\leqslant 33$, $-13\leqslant k\leqslant 13$, $-22\leqslant l\leqslant 22$	$-17\leqslant h\leqslant 17$, $-22\leqslant k\leqslant 22$, $-9\leqslant l\leqslant 9$	$-17\leqslant h\leqslant 18$, $-20\leqslant k\leqslant 20$, $-23\leqslant l\leqslant 22$
Total reflections	18527	18102	18636
Unique reflections	3911	3880	4178
R(int)	0.0711	0.0392	0.0389
Parameters/restraints	267/3	268/2	283/4
R_1 (all data)[a]	0.1005	0.0427	0.0467
R_1 ($I>2\sigma(I)$)	0.0608	0.0323	0.0295
wR_2 (all data)[b]	0.1568	0.0817	0.0841
wR_2 ($I>2\sigma(I)$)	0.1388	0.0775	0.0700
Max/min residual (e$^-$/Å^3)	0.531/−0.361	0.434/−0.500	0.616/−0.840
GOF	1.031	1.054	1.115

[a] $R_1 = \Sigma||F_o|-|F_c||/\Sigma|F_o|$.
[b] $wR_2 = \sum\{[w(F_o^2 - F_c^2)^2]/\sum[wF_o^2]^2\}^{1/2}$.

4. Results and discussion

4.1. Synthesis and spectral characterization

Compounds **1** and **2** were prepared cleanly under hydrothermal conditions via combination of zinc chloride, H_3BTC, and dpa with appropriate pH adjustment. Use of cadmium nitrate in a similar synthesis as **2** generated compound **3** as single-phase colorless blocks. Phase purity was judged as satisfactory by elemental analysis and powder X-ray diffraction via comparison with spectra predicted from the single-crystal structural determinations.

The infrared spectra of all complexes are consistent with the features evident in their single-crystal X-ray structures. Sharp, medium intensity bands in the range of ~1600–~1200 cm^{-1} were ascribed to stretching modes of the pyridyl rings of the dpa moieties [23] and the benzene rings within HBTC or BTC ligands. Features corresponding to pyridyl and benzene ring puckering mechanisms were evident in the region between 820 and 600 cm^{-1}. Asymmetric and symmetric C–O stretching modes of the benzenetricarboxylate moieties were evidenced by very strong, slightly broadened bands at ~1600 and ~1360 cm^{-1}. The $\Delta\nu$ values of ~240 cm^{-1} are consistent with monodentate coordination of the carboxylate units [24]. A band for the protonated uncoordinated carboxylate group in **1** was observed at 1716 cm^{-1}. Spectral features in the region of ~3400 cm^{-1} in all cases represent N–H stretching modes within the dpa ligands in **1**–**3**, and O–H stretching modes within **3**. The broadness of these latter spectral features is caused by significant hydrogen bonding pathways (vide infra).

4.2. Structural description of *[Zn(HBTC)$_2$(Hdpa)$_2$]* (*1*)

As revealed by single-crystal X-ray diffraction, the asymmetric unit of **1** contains a single divalent Zn atom on a crystallographic 2-fold axis, one singly protonated, monodentate HTBC ligand, and one monodentate dpa molecule protonated at its distal nitrogen locus. While protonated monodentate dpa ligands are relatively uncommon, they have been previously observed in molydate and sulfate complexes [17,19b]. The pH range for the reaction mixture during the synthesis of **1** was between 4.3 and 4.7, allowing equilibrium concentrations of $HBTC^{2-}$

dianions and $Hdpa^+$ cations as judged by the relative pK_a values for H_3BTC (3.14, 3.85, 4.55) and pK_b values for dpa (7.65, 8.27) [25]. A complete neutral molecule of $[Zn(HBTC)_2(Hdpa)_2]$ is shown with thermal ellipsoids in Fig. 1. The coordination environment is a distorted $[ZnN_2O_2]$ tetrahedron, with the two N donors and two O donors belonging to two separate Hdpa and HBTC ligands, respectively. The bond lengths and angles about Zn are standard for complexes of this type, and are listed in Table 2. Within the HBTC ligand, the three carboxylate moieties are twisted relative to the plane of the aromatic ring by ~17°, ~7°, and ~3°. The torsion angle between the pyridyl rings of the Hdpa ligand is ~14.2°. The hydrogen atom bound to carboxylate oxygen atom O5 was found during the structural determination. Protonation at this site is further corroborated by the longer C18–O5 bond length relative to C18–O4, indicating predominance of σ-bond characteristics.

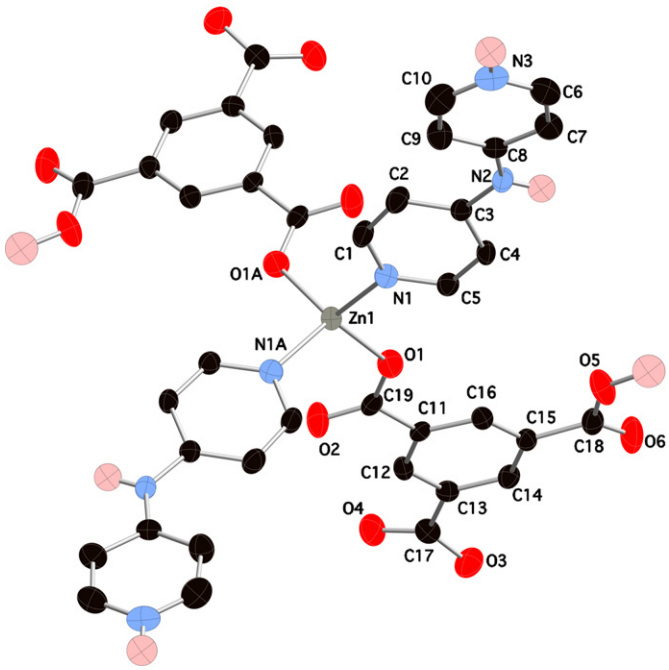

Fig. 1. Molecular species **1**, shown with thermal ellipsoids at 50% probability. Most hydrogen atoms have been omitted.

Table 2
Selected bond distance (Å) and angle (deg) data for **1**

Zn1–O1 (×2)	1.933(3)	$O1^{\#1}$–Zn1–O1	116.80(18)
Zn1–N1 (×2)	2.025(3)	$O1^{\#1}$–Zn1–N1	101.65(12)
O1–C19	1.283(5)	O1–Zn1–N1	114.78(12)
O2–C19	1.237(4)	$O1^{\#1}$–Zn1–$N1^{\#1}$	114.78(12)
O3–C17	1.264(5)	O1–Zn1–$N1^{\#1}$	101.65(12)
O4–C17	1.247(5)	N1–Zn1–$N1^{\#1}$	107.30(18)
O5–C18	1.321(5)		
O6–C18	1.199(5)		

Symmetry transformations to generate equivalent atoms: (#1) $-x+1$, y, $-z+1/2$.

Neighboring molecules of **1** stack via interdigitation along the *c* crystal direction and form pseudo 2-D slabs coincident with the *ac* crystal plane through two distinct supramolecular hydrogen bonding pathways (Fig. 2). The dpa amine subunits (N2–H2N) donate hydrogen bonds to unligated oxygen atoms of type O2, which belong to the monodentate carboxylate moieties attached to Zn. Also, the protonated carboxylate groups engage in hydrogen bonding donation to oxygen atoms of type O4, which are part of the unligated unprotonated carboxylate group. A third type of hydrogen bonding pattern subsequently serves to link juxtaposed pseudo 2-D slabs into the full 3-D crystal structure of **1**. Here, oxygen atoms of type O3, which belong to unligated and unprotonated carboxylate groups projecting above and below each 2-D slab, accept charge-separated hydrogen bonds from the protonated imine termini of the Hdpa ligands in neighboring slabs (Fig. 3). Data for all classical supramolecular interactions in **1** are given in Table 3.

4.3. Structural description of [Zn(BTC)(Hdpa)] (2)

The asymmetric unit of **2** consists of one divalent Zn atom, one fully deprotonated BTC and one protonated dpa ligand (Fig. 4). The elevated initial pH of the reaction mixture as compared to **1** causes full deprotonation of H_3BTC, while the reduction in this value over the course of

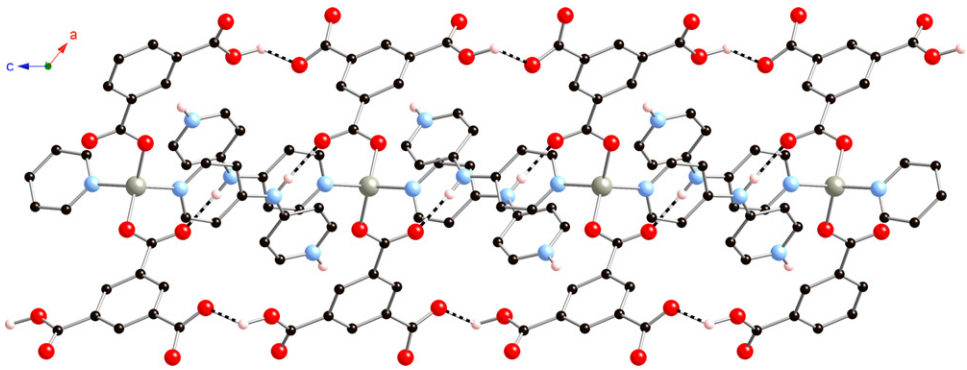

Fig. 2. Pseudo 2-D slab formed from the supramolecular interactions of neighboring molecules of **1**. Hydrogen bonding is shown as dashed lines.

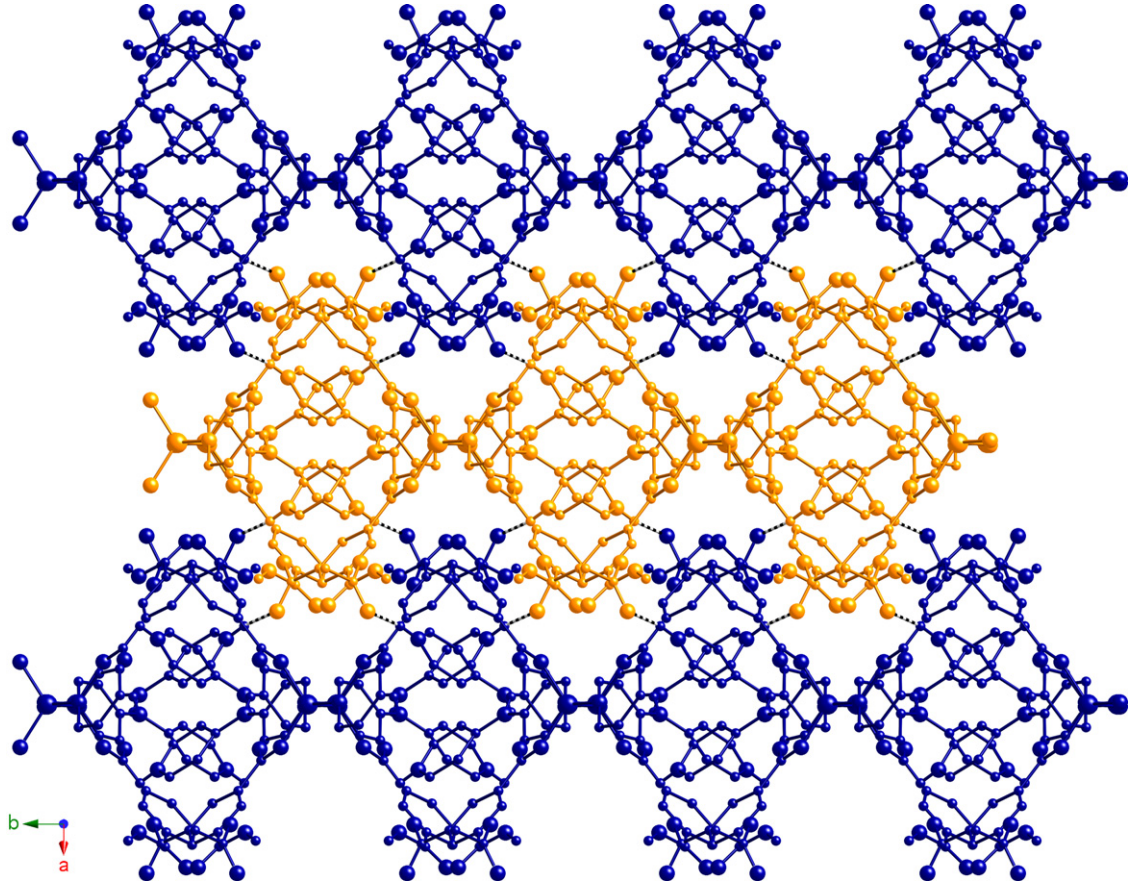

Fig. 3. Interaction of pseudo 2-D slabs in **1**, showing hydrogen bonding as dashed lines.

Table 3
Hydrogen bonding distance (Å) and angle (deg) data for **1**–**3**

D–H	*d*(H···A)	<DHA	*d*(D···A)	Symmetry transformation for *A*
1				
N2–H2N···O2	1.91(5)	153(3)	2.790(3)	$-x+1, -y, -z+1$
N3–H3N···O3	1.70(4)	163(6)	2.594(5)	$-x+3/2, y+3/2, -z+3/2$
O5–H5A···O4	1.85(4)	131(5)	2.543(5)	$x, -y-1, z-1/2$
2				
N2–H2N···O6	1.92(2)	168(2)	2.767(4)	$-x-1/2, -y+1/2, -z$
N3–H3N···O2	1.86(2)	143(2)	2.634(4)	$-x+1, -y, -z-1$
3				
N2–H2N···O6	1.93(3)	163(4)	2.788(4)	$x, -y+1, z-1/2$
N3–H3N···O5	1.74(3)	157(4)	2.593(4)	$x, y, z-1$
O7–H7A···O4	1.92(2)	175(4)	2.756(4)	$-x+1, y, -z+3/2$
O7–H7B···O1	1.92(3)	161(3)	2.724(4)	$-x+1, -y, -z+1$

the reaction permits the presence of an equilibrium concentration of the $Hdpa^+$ cations required for charge neutrality in **2**. As in **1**, the coordination environment about Zn is best described as distorted tetrahedral, however with a $[ZnO_3N]$ arrangement in this case. Pertinent bond length and angle information for **2** is given in Table 4. The kinked monodentate Hdpa ligand is twisted to a much greater extent (~36.5°) than in **1** in order to maximize its supramolecular interactions (vide infra).

Junction of neighboring coordination units through two monodentate carboxylate units of a single BTC ligand gives rise to 1-D [Zn(BTC)(Hdpa)] serpentine chains running along the *c* crystal direction. The carboxylate groups involved in the construction of this chain motif (O1/C17/O2, group *A*; O3/C18/O4, group *B*) are rotated by ~15°

and ~9° relative to the plane of the BTC aromatic ring. The Zn–Zn distance through the *A* and *B* carboxylate groups of a BTC ligand measures 9.034(2) Å. Adjacent chains then link covalently through a third type of monodentate carboxylate moiety (O5/C19/O6, group *C*) to build an undulating 2-D coordination polymeric slab substructure (Fig. 5). In order to achieve this connectivity pattern, carboxylate group *C* is required to contort significantly (~32°) from the plane of the BTC aromatic ring. As a result, the interchain Zn–Zn distance (6.715(2) Å) is shorter than the intrachain contact. Within the layer, each Zn atom is connected to five others through three different triply monodentate BTC ligands, while each BTC unit acts as an exotridentate connector to three different Zn atoms. The Zn–ring centroid distances through carboxylate groups *A*, *B*, and *C* measure 5.52, 4.11, and 5.53 Å, respectively. The coordination polymeric nature of **2** can be viewed as 4.8^2 3-connected network 2-D slabs constructed from the junction of 16-membered $[(ZnOC_5O)_2]$ rings with 32-membered $[(ZnOC_5O)_4]$ ellipsoids, evident from Fig. 5. As defined by the Zn–Zn and H14–H14 through-space contacts, the distances across the 16-membered ring patterns measure 6.715(2) Å × 3.655(2) Å. The smallest and largest through-space Zn–Zn distances of 18.082(2) and 4.431(1) Å demarcate the dimensions of the intralayer 32-membered ellipsoids.

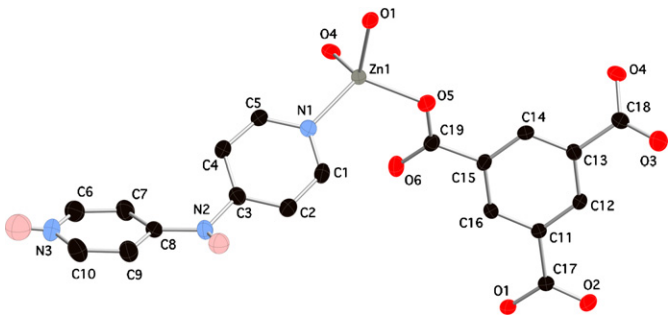

Fig. 4. Asymmetric unit of **2**, shown with thermal ellipsoids at 50% probability. Most hydrogen atoms have been omitted.

Table 4
Selected bond distance (Å) and angle (deg) data for **2**

Zn1–O5$^{\#1}$	1.955(2)	O5$^{\#1}$–Zn1–O4$^{\#2}$	114.21(11)
Zn1–O4$^{\#2}$	1.967(2)	O5$^{\#1}$–Zn1–O1	100.42(9)
Zn1–O1	1.981(3)	O4$^{\#2}$–Zn1–O1	109.31(7)
Zn1–N1	2.031(3)	O5$^{\#1}$–Zn1–N1	113.41(9)
O1–C17	1.275(3)	O4$^{\#2}$–Zn1–N1	104.47(10)
O2–C17	1.242(3)	O1–Zn1–N1	115.34(9)
O3–C18	1.233(3)		
O4–C18	1.285(3)		
O5–C19	1.277(3)		
O6–C19	1.249(3)		

Symmetry transformations to generate equivalent atoms: (#1) $-x+2$, $y-1/2$, $-z+1/2$; (#2) $-x$, $-y+1$, $-z+1$.

In addition to the information contained in the covalent bonding in this system, structure direction is assisted by intralayer hydrogen bonding between the central amine units of the kinked Hdpa ligands and unligated oxygen atoms (O6) belonging to carboxylate unit of type *C*.

Adjacent slabs are then connected into the pseudo 3-D structure of **2** (Fig. 6) through the pendant protonated Hdpa ligands which project into the interlamellar regions

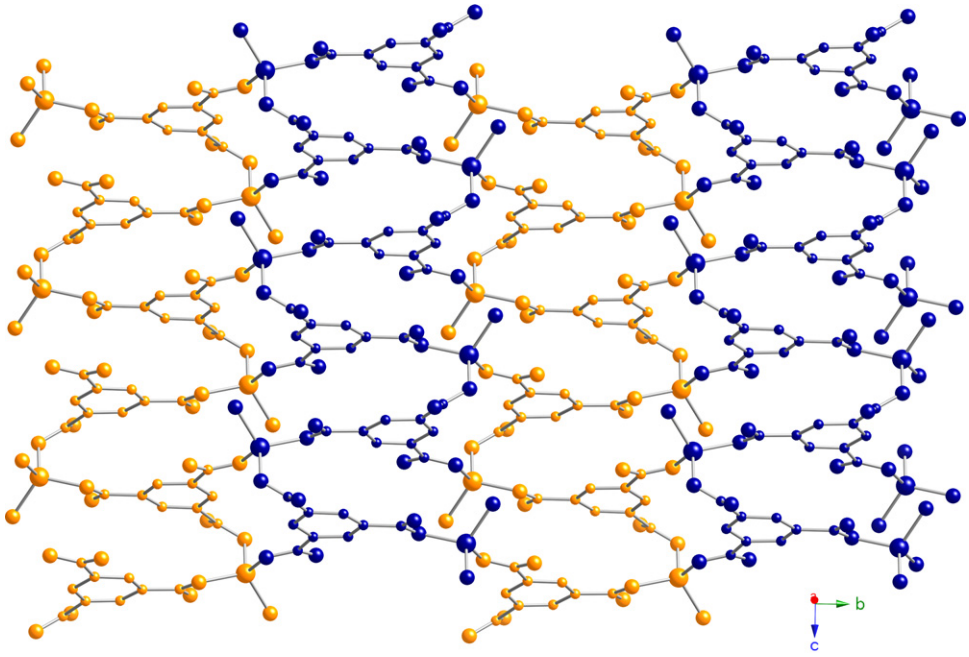

Fig. 5. A single 4.8^2 3-connected [Zn(BTC)(Hdpa)] layer in **2**, formed from the junction of 1-D chain motifs through carboxylate group *C*. Only the N atoms of the Hdpa ligands are shown for clarity.

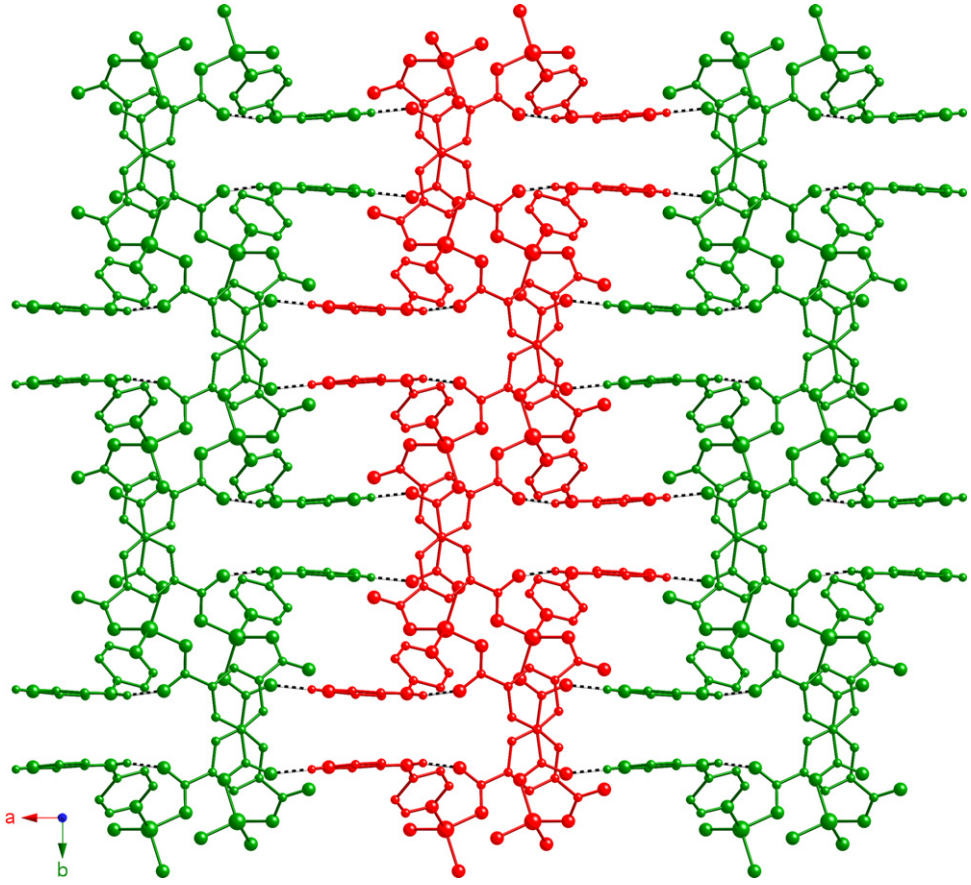

Fig. 6. Interaction of 2-D layers in **2**, with Hdpa-promoted intralayer and interlayer hydrogen bonding shown as dashed lines.

and engage in hydrogen bonding with unligated carboxylate oxygen atoms denoted by O2, part of carboxylate group *A*. The closest Zn–Zn distance between neighboring 2-D slabs is 9.360(2) Å. Supramolecular contact information for **2** is given in Table 3.

4.4. Structural description of [Cd(BTC)(H$_2$O)(Hdpa)] (**3**)

The asymmetric unit of **3** (Fig. 7) consists of a single cadmium atom, one fully deprotonated BTC and one protonated pendant Hdpa ligand, as well as a single bound water molecule. As is the case for **2**, the initial basic reaction conditions allow full deprotonation of H_3BTC. Equilibrium amounts of charge-compensating $Hdpa^+$ cations could then subsequently form as the pH of the reaction mixture decreases. The coordination environment is a distorted octahedral [CdO_5N] pattern, with four of the oxygen atoms belonging to carboxylate moieties of three distinct BTC ligands. The coordination sphere is rounded out by a nitrogen donor from the monodentate protonated dpa ligand and an aquo ligand, which are disposed in a *cis* manner to each other. The longer bond lengths in **3** and increased coordination number, as compared with **2**, are consistent with the larger ionic radius of Cd^{2+} relative to Zn^{2+} [26]. Selected geometric parameters for **3** are given in Table 5.

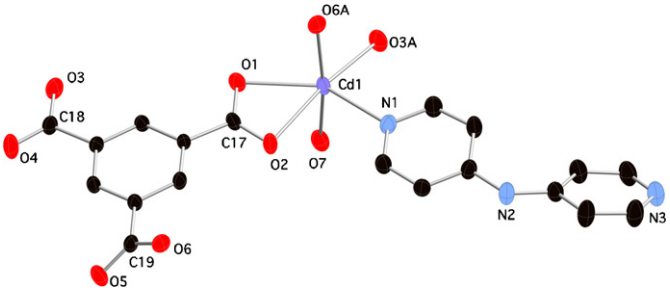

Fig. 7. Asymmetric unit of **3** with thermal ellipsoids at 50% probability. Hydrogen atoms have been omitted for clarity.

Within a single BTC unit, one of its carboxylates (group *A*, marked by O1/C17/O2) binds to Cd in a chelating fashion, while the other two (O3/C18/O4, group *B*; O5/C19/O6, group *C*) display monodentate binding modes. The bite angle at Cd of chelating carboxylate *A* is 55.21(8)°; this group binds to Cd in a slightly asymmetric fashion, with the Cd–O1 distance 0.02 Å shorter than Cd–O2. The Cd-to-BTC ring centroid distances through carboxylate groups *A*, *B*, and *C* are ~5.62, ~5.81, and ~4.52 Å, respectively.

Through the two monodentate carboxylate termini (groups *B* and *C*) of the exotridentate BTC ligands, adjacent Cd atoms are connected into rippled 1-D chain

Table 5
Selected bond distance (Å) and angle (deg) data for **3**

Cd1–O3$^{\#1}$	2.210(2)	N1–Cd1–O6$^{\#2}$	94.37(9)
Cd1–N1	2.318(3)	O3$^{\#1}$–Cd1–O7	91.28(10)
Cd1–O6$^{\#2}$	2.350(3)	N1–Cd1–O7	94.52(10)
Cd1–O7	2.354(3)	O6$^{\#2}$–Cd1–O7	171.09(8)
Cd1–O1	2.371(2)	O3$^{\#1}$–Cd1–O1	130.18(9)
Cd1–O2	2.392(2)	N1–Cd1–O1	143.08(9)
O1–C17	1.269(4)	O6$^{\#2}$–Cd1–O1	85.24(9)
O2–C17	1.257(4)	O7–Cd1–O1	87.91(9)
O3–C18	1.262(4)	O3$^{\#1}$–Cd1–O2	172.18(9)
O4–C18	1.240(4)	N1–Cd1–O2	88.46(9)
O5–C19	1.249(4)	O6$^{\#2}$–Cd1–O2	97.66(9)
O6–C19	1.270(4)	O7–Cd1–O2	83.01(9)
		O1–Cd1–O2	55.21(8)
O3$^{\#1}$–Cd1–N1	86.66(10)	O2–C17–O1	121.8(3)
O3$^{\#1}$–Cd1–O6$^{\#2}$	88.81(10)	O4–C18–O3	125.1(3)
		O5–C19–O6	123.8(3)

Symmetry transformations to generate equivalent atoms: (#1) $x, -y, z-1/2$; (#2) $-x+1/2, -y+1/2, -z+1$.

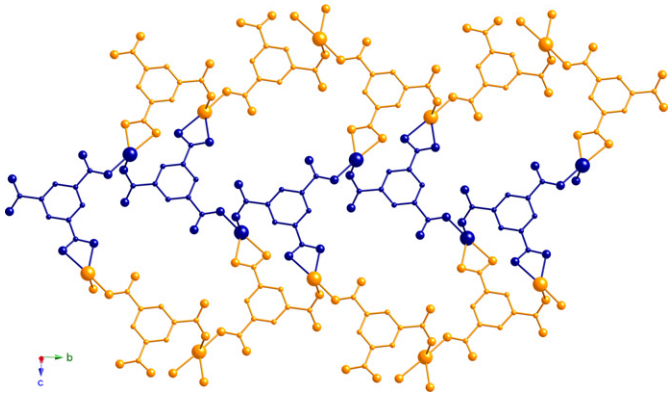

Fig. 8. Undulating 2-D 4.8^2 3-connected network layer in **3**.

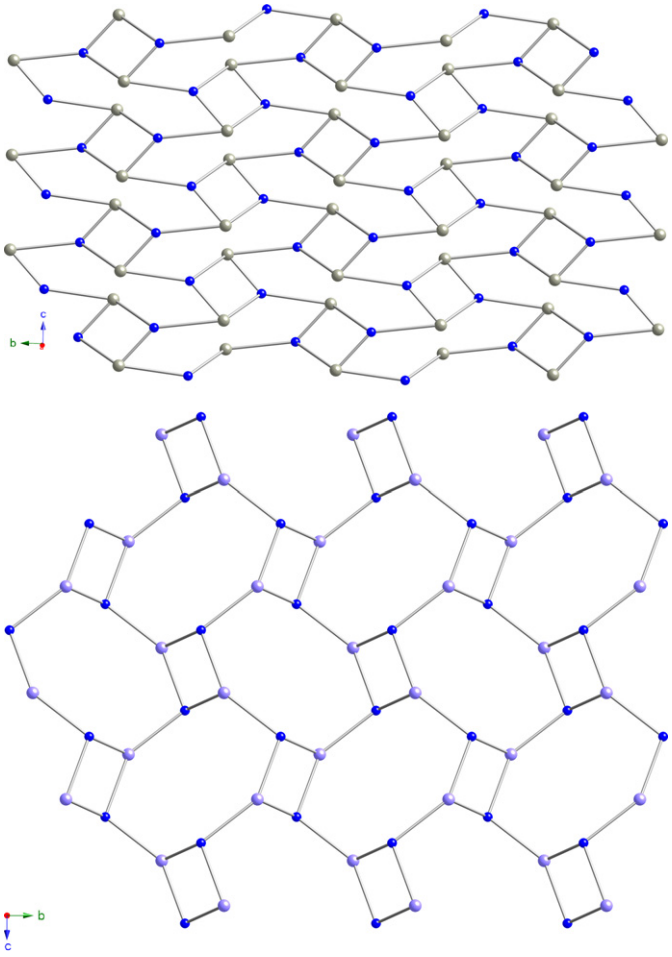

Fig. 9. 4.8^2 3-connected networks in **2** (top) and **3** (bottom). In both cases only the metal atoms and BTC ring centroids are shown.

motifs (Cd–Cd distances = 9.220(1) and 9.371(1) Å), which in turn link to neighboring chains through the chelating BTC carboxylate unit (group *A*) to construct undulating 2-D layers parallel to the *bc* crystal plane, in a 4.8^2 3-connected network with ring and ellipsoid structural patterns similar to that observed in **2** (Fig. 8). However, the chelating carboxylate binding mode and aquo ligand necessitated by the preference for octahedral coordination in **3** acts to foster geometric alterations of these patterns. The 16-membered $[(CdOC_5O)_2]$ rings measure 7.746(1) Å × 3.833(1) Å, as defined by through-space Cd–Cd and H16–H16 distances. The 32-membered $[(CdOC_5O)_4]$ ellipsoids are substantially less oblate than the related features in **2**, with its cross-channel Cd–Cd distances measuring 11.862(1) and 14.315(1) Å. A side-by-side framework perspective of the 4.8^2 networks in **2** and **3** (Fig. 9), where the metal atoms and ring centroids are depicted as 3-connected nodes, highlights these coordination geometry-driven alterations. The extra width in the ellipsoidal cavities allows the Hdpa ligands in **3** to lie largely within the confines of the layer motifs (Fig. 10), held in place by supramolecular hydrogen bonding between both N–H subunits and oxygen atoms belonging to carboxylate group *C* in two different BTC ligands. The Hdpa ligands exhibit an inter-ring torsion angle of 28.2° to maximize these attractive interactions.

Because the aqua ligands in **3** are disposed *cis* to the Hdpa units oriented within the layers, they project above and below the layer plane and permit aggregation of abutting 2-D coordination polymer units through hydrogen bonding to oxygen atoms belonging to BTC carboxylate units of type *A* and *B* (see Table 3 for geometric details). The confinement of the sterically bulky pendant Hdpa ligands to the layer subunits allows close approach of the 2-D coordination polymer subunits in **3** (Fig. 11), with an interlayer Cd–Cd contact distance of 5.052(1) Å, almost 4 Å nearer than in **2**.

4.5. Thermal behavior

Thermogravimetric analysis was performed on ground samples of **1**–**3** to ascertain their thermal robustness and

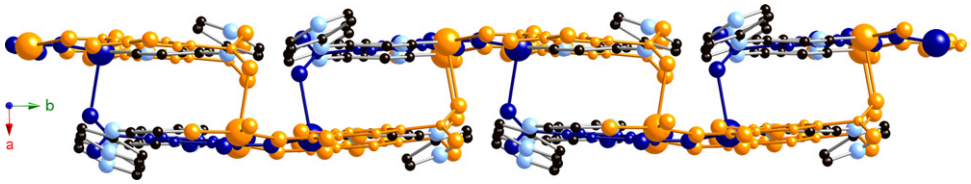

Fig. 10. Side view of the 2-D layer motif in **3**, highlighting the in-plane orientation of the pendant Hdpa ligands.

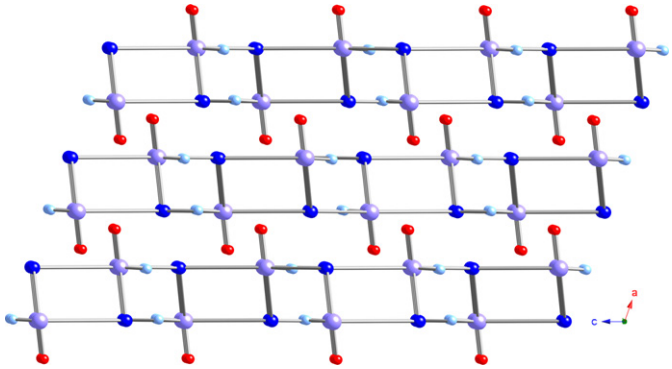

Fig. 11. Stacking of 2-D slab motifs in **3**, shown in a framework perspective. The aquo ligands engaged in interlayer hydrogen bonding can be seen projecting above and below each individual layer.

decomposition behavior. Complex **1** underwent a slow mass loss of 4.8% between 100 and 360 °C, corresponding to possible decarboxylation of one of its coordinated BTC ligands (5.3% calc'd). A precipitous mass loss of 86.6% between 375 and 550 °C indicated complete decomposition by elimination of all Hdpa and intact and decarboxylated BTC ligands (86.5% predicted). The remnant of 9.7% of the original mass corresponds well to the deposition of ZnO (9.9% calc'd). Compound **2** manifested high thermal stability, with virtually no mass loss occurring until 375 °C. Between this temperature and 475 °C a mass loss of 50.2% was observed, roughly consistent with the expulsion of Hdpa (38.7% calc'd) and a single equivalent of CO_2 due to decarboxylation of BTC (9.9% calc'd). A slow mass loss of 24.4% took place between 475 and 900 °C, indicative of continued decarboxylation and combustion of the BTC ligands. The 25.4% remnant at the instrument temperature limit of 900 °C indicates a likely admixture of ZnO (18.2% calc'd) along with some uncombusted organic material. The cadmium derivative **3** exhibited dehydration between 200 and 300 °C (4.6% mass loss, 3.5% predicted), reflective of aqua ligand coordination. Loss of CO_2 due to decarboxylation then occurred between 300 and 350 °C (15.5% mass loss observed, 17.2% calc'd for two equivalents of CO_2). Combustion of all organics was complete by 600 °C, with a mass loss of 54.5% consistent with expulsion of Hdpa and a benzoate unit. The final remnant of 24.9% of the original mass is consistent with a formulation of CdO (25.2% theoretical). TGA traces for **1**–**3** are shown in Figures S1–S3, respectively.

4.6. Luminescent properties

Irradiation of complexes **1**–**3** with ultraviolet light ($\lambda = 300$ nm) in the solid state resulted in blue–violet visible light emission in all cases. Slightly different emission maxima (**1**, λ_{max}~375 nm; **2**, λ_{max}~400 nm; **3**, λ_{max}~390 nm) were observed (Fig. 12). These emissions likely originate from ligand-centered π–π^* or π–n electronic transitions within either the aromatic ring systems of the BTC or dpa ligands. Ligand-centered blue light luminescence is a commonly encountered feature within d^{10}-metal coordination polymers [27]. The shifts in emission maxima likely represent subtle differences in ligand-based molecular orbital energy levels due to variances in carboxylate binding mode, coordination geometry, and bond lengths to the metal cations. While deliberate tailoring of emission properties within d^{10} coordination polymer systems with aromatic ligands remains an elusive goal, this class of materials may provide functional luminescent solids for light-emitting diode applications.

5. Conclusions

Hydrothermal synthesis has permitted the self-assembly of three divalent d^{10}-metal complexes incorporating both BTC and dpa ligands. In the zinc case, the molecular species $[Zn(Hdpa)_2(HBTC)_2]$ (**1**) and the 2-D 4.8^2 layered material [Zn(Hdpa)(BTC)] (**2**) were cleanly prepared depending on the initial pH of the reaction mixture. In both cases, the protonated pendant Hdpa ligand serves to connect adjacent neutral units into the full crystal structures through extensive supramolecular hydrogen bonding interactions. Employment of a cadmium precursor results in the 2-D 4.8^2 layered coordination polymer $[Cd(Hdpa)(BTC)(H_2O)]$ (**3**). While the layered motifs in **2** and **3** display the same topological connectivity, the expansion of the coordination geometry in **3** instigates a dramatic shift in both the layer morphology and the supramolecular interaction pathways, resulting in a denser material. Both the covalent and hydrogen bonding pathways promote a high degree of thermal stability, even in the case of the "molecular" species **1**. All three materials display blue–violet visible light luminescence upon excitation with ultraviolet light, reinforcing the promise of zinc and cadmium coordination polymeric complexes in light-emitting device applications. Fruitful efforts to prepare other dpa-containing coordination polymers continue in

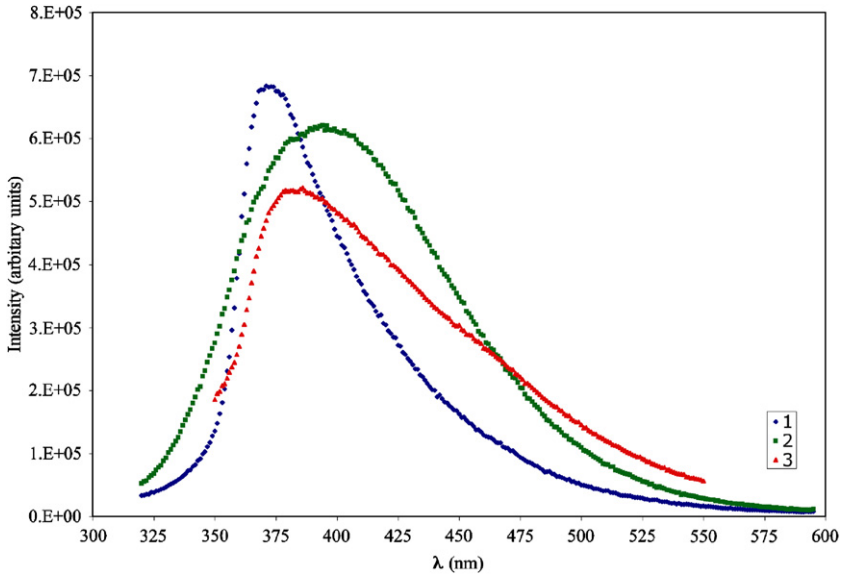

Fig. 12. Emission spectra of **1**–**3**.

our laboratory, taking advantage of this ligand's unique covalent bonding and supramolecular interaction patterns.

Acknowledgments

We thank Michigan State University for funding this work. M.A.B. is grateful for the MSU Quality Fund Undergraduate Research Program for financial support. We are indebted to Amanda Smeigh for helpful discussions, Troy Knight for acquisition of the emission spectra, Dr. James McCusker for use of the fluorimeter, and Dr. Rui Huang for elemental analysis. We thank the reviewers for the kind suggestions to improve the manuscript.

Appendix A. Supplementary materials

Supplementary data associated with this article can be found in the online version at doi:10.1016/j.jssc.2007.04.010.

References

[1] (a) H. Li, M. Eddaoudi, M. O'Keeffe, O.M. Yaghi, Nature 402 (2005) 276;
(b) R. Matsuda, R. Kitaura, S. Kitagawa, Y. Kubota, R.U. Belosludov, T.C. Kobayashi, H. Sakamoto, T. Chiba, M. Takata, Y. Kawazoe, Y. Mita, Nature 436 (2005) 238;
(c) L. Pan, D. Holson, L.R. Ciemnolonski, R. Heddy, J. Li, Angew. Chem. Int. Ed. 46 (2006) 616;
(d) N.L. Rosi, J. Eckert, M. Eddaoudi, D.J. Vodak, J. Kim, M. O'Keeffe, O.M. Yaghi, Science 300 (2003) 1127;
(e) M. Dinca, A.F. Yu, J.R. Long, J. Am. Chem. Soc. 128 (2006) 8904;
(f) G. Ferey, M. Latroche, C. Serre, F. Millange, T. Loiseau, A. Percheron-Guegan, Chem. Commun. (2003) 2976;
(g) X. Zhao, B. Xiao, A.J. Fletcher, K.M. Thomas, D. Bradshaw, M.J. Rosseinsky, Science 306 (2004) 1012.

[2] (a) J.S. Seo, D. Whang, H. Lee, S.I. Jun, J. Oh, Y.J. Jeon, K. Kim, Nature 404 (2000) 982;
(b) B. Chen, C. Liang, J. Yang, D.S. Contreras, Y.L. Clancy, E.B. Lobkovsky, O.M. Yaghi, S. Dai, Angew. Chem. Int. Ed. 45 (2006) 1390.

[3] (a) Q.-R. Fang, G.-S. Zhu, M. Xue, J.-Y. Sun, S.-L. Qiu, Dalton Trans. (2006) 2399;
(b) X.-M. Zhang, M.-L. Tong, H.K. Lee, X.-M. Chen, J. Solid State Chem. 160 (2001) 118;
(c) O.M. Yaghi, H. Li, T.L. Groy, Inorg. Chem. 36 (1997) 4292.

[4] (a) N. Guillou, P.M. Forster, Q. Gao, J.S. Chang, M. Nogues, S.-E. Park, A.K. Cheetham, G. Ferey, Angew. Chem. Int. Ed. 40 (2001) 2831;
(b) C.-D. Wu, A. Hu, L. Zhang, W. Lin, J. Am. Chem. Soc. 127 (2005) 8940;
(c) H. Han, S. Zhang, H. Hou, Y. Fan, Y. Zhu, Eur. J. Inorg. Chem. 8 (2006) 1594;
(d) W. Mori, S. Takamizawa, C.N. Kato, T. Ohmura, T. Sato, Micropor. Mesopor. Mater. 73 (2004) 15.

[5] (a) S. Zang, Y. Su, Y. Li, Z. Ni, Q. Meng, Inorg. Chem. 45 (2006) 174;
(b) L. Wang, M. Yang, G. Li, Z. Shi, S. Feng, Inorg. Chem. 45 (2006) 2474;
(c) S. Wang, Y. Hou, E. Wang, Y. Li, L. Xu, J. Peng, S. Liu, C. Hu, New J. Chem. 27 (2003) 1144;
(d) L.G. Beauvais, M.P. Shores, J.R. Long, J. Am. Chem. Soc. 122 (2000) 2763;
(e) H. Jianghua, Y. Jihong, Z. Yuetao, P. Qinhe, X. Ruren, Inorg. Chem. 44 (2005) 9279.

[6] M. Eddaoudi, H. Li, O.M. Yaghi, J. Am. Chem. Soc. 122 (2000) 1391.

[7] O.M. Yaghi, H. Li, T.L. Groy, J. Am. Chem. Soc. 118 (1996) 9096.

[8] O.M. Yaghi, C.E. Davis, G. Li, H. Li, J. Am. Chem. Soc. 119 (1997) 2861.

[9] Q. Fang, G. Zhu, M. Xue, J. Sun, F. Sun, S. Qiu, Inorg. Chem. 45 (2006) 3582.

[10] M.J. Plater, M.R.St.J. Foreman, E. Coronado, C.J. Gomez-Garcia, A.M.Z. Slawin, J. Chem. Soc., Dalton Trans. (1999) 4209.

[11] X. Li, R. Cao, D. Sun, D. Yuan, W. Bi, X. Li, Y. Wang, J. Molec. Struct. 694 (2004) 205.

[12] P.-K. Chen, Y.-X. Che, Y.-M. Li, J.-M. Zheng, J. Solid State Chem. 179 (2006) 2656.

[13] Z. Shi, G. Li, L. Wang, L. Gao, X. Chen, J. Hua, S. Feng, Crystal Gr. Des. 4 (2004) 25.
[14] X.-F. Zhou, B.-Y. Lou, D.-Q. Yuan, Y.-Q. Xu, F.-L. Jiang, M.-C. Hong, Inorg. Chim. Acta 358 (2005) 3057.
[15] (a) J. Zhang, Y.-B. Chen, S.-M. Chen, Z.-J. Li, J.-K. Cheng, Y.-G. Yao, Inorg. Chem. 45 (2006) 3161;
(b) F.A. Almeida Paz, J. Klinowski, Inorg. Chem. 43 (2004) 3882.
[16] M.R. Montney, S. Mallika Krishnan, N.M. Patel, R.M. Supkowski, R.L. LaDuca, Crystal Gr. Des 7 (2007) (in press) doi:10.1021/cg070008l.
[17] P.J. Zapf, R.L. LaDuca, R.S. Rarig, K.M. Johnson, J. Zubieta, J. Inorg. Chem. 37 (1998) 3411.
[18] R. LaDuca, M. Laskoski, J. Zubieta, J. Chem. Soc., Dalton Trans. (1999) 3467.
[19] (a) D.B. Cordes, L.R. Hanton, M.D. Spicer, Inorg. Chem. 45 (2006) 7651;
(b) D.B. Cordes, L.R. Hanton, M.D. Spicer, Crystal Gr. Des. 7 (2007) 328.
[20] SAINT, Software for Data Extraction and Reduction, Version 6.02, Bruker AXS, Inc., Madison, WI, 2002.
[21] SADABS, Software for Empirical Absorption Correction, Version 2.03, Bruker AXS, Inc., Madison, WI, 2002.
[22] G.M. Sheldrick, SHELXTL, Program for Crystal Structure Refinement, University of Gottingen, Gottingen, Germany, 1997.
[23] M. Kurmoo, C. Estournes, Y. Oka, H. Kumagai, K. Inoue, Inorg. Chem. 44 (2005) 217.
[24] K. Nakamoto, Infrared Spectra and Raman Spectra of Inorganic and Coordination Compounds, Wiley, New York, 1986.
[25] pK_a and pK_b values and microspecies equilibrium concentration values were calculated using the *MarvinBeans* program, Version 4.1.6., available at 〈http://www.chemaxon.com〉.
[26] R.D. Shannon, Acta Crystallogr. A 32 (1976) 751.
[27] (a) J. Tao, J.X. Shi, M.L. Tong, X.X. Zhang, X.M. Chen, Inorg. Chem. 40 (2001) 6328;
(b) J. Tao, M.L. Tong, J.X. Shi, X.M. Chen, S.W. Ng, Chem. Commun. (2000) 2043;
(c) J.C. Dai, X.T. Wu, Z.Y. Fu, C.P. Cui, S.M. Hu, W.X. Du, L.M. Wu, H.H. Zhang, R.Q. Sun, Inorg. Chem. 41 (2002) 1391;
(d) W. Chen, J.Y. Wang, C. Chen, Q. Yue, H.M. Yuan, J.S. Chen, S.N. Wang, Inorg. Chem. 42 (2003) 944;
(e) N. Hao, E. Shen, Y.B. Li, E.B. Wang, C.W. Hu, L. Xu, Eur. J. Inorg. Chem. (2004) 4102.